

## Article

# Comparison of Commercial REBCO Tapes Through Flux Pinning Energy

Masood Rauf Khan <sup>1</sup>, Antonio Leo <sup>1,\*</sup>, Andrea Masi <sup>2</sup>, Achille Angrisani Armenio <sup>2</sup>, Andrea Augieri <sup>2</sup>, Giuseppe Celentano <sup>2</sup>, Armando Galluzzi <sup>3</sup>, Massimiliano Polichetti <sup>3</sup>, Angela Nigro <sup>3</sup>, and Gaia Grimaldi <sup>1,\*</sup>

- <sup>1</sup> National Research Council Institute for Superconductors, INnovative Materials, and Devices, CNR-SPIN, c/o, University of Salerno, Via Giovanni Paolo II, 132, 84084 Fisciano, Italy; masoodrauf.khan@spin.cnr.it
- <sup>2</sup> ENEA—Italian National Agency for New Technologies, Energy and Sustainable Economic Development, C.R. Frascati, 00044 Frascati, Italy; andrea.masi@enea.it (A.M.); achille.angrisaniarmenio@enea.it (A.A.A.); andrea.augieri@enea.it (A.A.); giuseppe.celentano@enea.it (G.C.)
- <sup>3</sup> Physics Department 'E. R. Caianiello', University of Salerno, Via Giovanni Paolo II, 132, 84084 Fisciano, Italy; agalluzzi@unisa.it (A.G.); mpolichetti@unisa.it (M.P.); anigro@unisa.it (A.N.)
- \* Correspondence: antonio.leo@spin.cnr.it (A.L.); gaia.grimaldi@spin.cnr.it (G.G.)

**Abstract:** This work presents a comparison of different commercial tapes belonging to the second-generation High-Temperature Superconductors (2G HTS) produced by SuNAM Co., Ltd., SuperOx, and Shanghai Superconductors Technology Co., Ltd. (SST) companies. The aim is to investigate pinning mechanisms responsible for best performances, looking at the anisotropy of the irreversibility field and of the flux pinning energy. The irreversibility line states the upper limit of current-carrying capacity, whereas the flux pinning energy explores the ability of material defects to act as weak collectively or strong single vortex pinning centers. All investigated samples have artificial pinning centers (APCs) included in the superconducting matrix: BHO-doped EuBCO for SST, Y<sub>2</sub>O<sub>3</sub> in YBCO for SuperOx, and Gd<sub>2</sub>O<sub>3</sub> particles trapped in GdBCO for SuNAM. Resistive transition curves were measured in high magnetic fields up to 16 T for magnetic field orientations parallel and perpendicular to the tape surface. We found that the anisotropy of SST tape shows an overall independence both on temperature and magnetic field, while the other two samples show a more complex behavior. This leads to the conclusion that properly engineered APC optimization in coated conductors can further reduce anisotropy of superconducting properties.

**Keywords:** flux pinning energy; irreversibility field; commercial REBCO tape; magnetoresistance measurements



**Citation:** Khan, M.R.; Leo, A.; Masi, A.; Angrisani Armenio, A.; Augieri, A.; Celentano, G.; Galluzzi, A.; Polichetti, M.; Nigro, A.; Grimaldi, G. Comparison of Commercial REBCO Tapes Through Flux Pinning Energy. *Crystals* **2024**, *14*, 1017. <https://doi.org/10.3390/cryst14121017>

Academic Editor: Arcady Zhukov

Received: 5 August 2024

Revised: 15 November 2024

Accepted: 19 November 2024

Published: 23 November 2024



**Copyright:** © 2024 by the authors. Licensee MDPI, Basel, Switzerland. This article is an open access article distributed under the terms and conditions of the Creative Commons Attribution (CC BY) license (<https://creativecommons.org/licenses/by/4.0/>).

## 1. Introduction

In recent times, coated conductor (CC) based on Rare Earth Barium Copper Oxide (REBCO) superconductors have attracted significant attention for their outstanding performance in high-field and high-power applications given their ability to maintain high current density in high magnetic fields in a temperature range where conventional superconductors fall short [1–5]. That's why REBCO superconductors already are or will shortly be employed in the manufacturing of cables, magnets, transformers, fault current limiters, and rotating machines. Their ability to carry current at extremely high densities enables them to not only reduce energy losses but also significantly decrease the weight and size of devices in various applications [6–9].

REBCO-coated conductors are produced by advanced technological processes, typically involving multiple steps that require different fabrication techniques and sophisticated equipment. By the way, the whole fabrication process must be reliable, scalable, and possibly open to improvements in order to produce the long-length tapes needed for the majority of applications [10–12]. Thus, REBCO CC tapes can be seen as a complex system with a

multilayered structure where a series of buffer layers facilitate a kind of epitaxial growth of the REBCO superconducting layer with a degree of crystallographic orientations that realizes the functional properties of the superconducting tapes [9,13,14], preserving and possibly improving the maximum electrical current that can flow through a superconductor, that is the critical current,  $I_c$ , and its resilience against high magnetic fields [15–18]. Several companies manufacture REBCO CC tapes, each employing specific combinations of materials and fabrication techniques. These manufacturing processes offer a variety of conductors with different properties, establishing REBCO CC tapes as a leading High-Temperature Superconductors (HTS) on the commercial market [19–26].

Critical parameters, particularly the external magnetic field, have a considerable influence on the superconductor critical current. The significant current decrease with increasing magnetic field is due to the dissipative motion of the Abrikosov vortices driven by the Lorentz force rising from the combined action of the current flowing through the superconductor and of the externally applied, or self-induced, magnetic field. An effective way to reduce this critical current drop is to strengthen the material capability to pin the vortices. A suitable way to improve pinning properties is achieved by introducing defects into the superconductor, which anchor the non-superconducting cores of the vortices and which do not deplete significantly critical temperature at the same time [27]. The effectiveness of vortex pinning is significantly influenced by microstructural defects [28,29]. Defects that result from high-energy particle irradiation of the superconductor [30–32], deliberate inclusion of extrinsic compounds [33–37], and intrinsic defects produced during the manufacturing process can all function as effective pinning centers. These defects interact with the vortices while vortices are interacting with each other, establishing a complex pinning landscape essential for maintaining high critical current under varying magnetic fields and temperatures [38,39].

Given the important role of pinning properties, it is important to better understand and characterize all the mechanisms leading to these properties in commercially available superconducting tapes [40,41]. By studying the flux pinning energy behavior, it is possible to add valuable information to this knowledge, which in turn is critical to improving the performance of superconducting devices and ensuring their reliability in real-world applications [40–43]. That is why the present study aims to investigate the pinning properties, and in particular flux pinning energy and its anisotropy in high applied magnetic fields of coated conductors produced by SuNAM and SuperOx. Through detailed electrical transport measurements, we seek to elucidate the performance and operational capabilities of these coated conductors across a range of magnetic fields and temperatures. Our findings will contribute to a broader understanding of vortex dynamics and pinning mechanisms in commercial REBCO tapes, providing valuable insights for the development and application of superconducting technologies.

## 2. Materials & Methods

### 2.1. Samples

In this study, we focused on analyzing samples from SuperOx Japan LLC (SuperOx Japan LLC, Sagamihara Incubation Center (SIC-3), Sagamihara, Kanagawa 1880-2 Kamimizo, Chuo-ku 252-0243, Japan) and SuNAM Co., Ltd. (SuNAM Co., Ltd., 52 Seungryang-gil, AnSeong, Republic of Korea) and comparing them with Shanghai Superconductors Technology Co., Ltd. (Shanghai Superconductor Technology Co., Ltd. (SST), 781 Kangwei Road, Pudong District, Shanghai, China) ones, very recently investigated [41]. In addition, we include a plain YBCO film just studied recently as reference material [44]. Commercially coated conductors are built on two fundamental components: a biaxially textured template and an epitaxial REBCO layer. The textured template, consisting of a flexible metallic tape coated with a multifunctional oxide barrier, is achieved through one of two methods: deforming the metal substrate using rolling-assisted biaxially textured substrate technology (RABiTS) or texturing the buffer layers deposited on the metal substrate via ion beam assisted deposition (IBAD) and its variant, alternating beam assisted deposition (ABAD) [24,27].

The epitaxial REBCO layer is produced using either chemical or physical deposition methods. Chemical routes include metal organic deposition (MOD) and metal organic chemical vapor deposition (MOCVD), while physical routes encompass pulsed laser deposition (PLD) and reactive co-evaporation (RCE). The deposition and conversion of precursors into the REBCO layer can occur in a single step (in situ process), as seen with MOCVD and PLD, or in two steps (ex situ process), as with MOD and RCE [10,11,24,27].

To complete the conductor, a few micrometers of a standard high-performance electrical and thermal conductor, such as silver or copper, are added for moisture protection and for thermal and electrical stabilization.

As anticipated, in this work we consider three samples in the form of coated conductors. The first sample is a BHO-doped EuBCO 4 mm wide tape produced by Shanghai Superconductor Technology Co., Ltd. (see [41] for additional details); in the following, we will refer to this sample as SST. The second sample is a 4 mm wide tape from SuNAM (batch #SCN-04-200) based on GdBCO fabricated using the RCE-DR (Reactive Co-Evaporation by Deposition and Reaction) process on IBAD substrate, with tapped  $Gd_2O_3$  particles; in the following we will refer to it as SuNAM. Both these samples are fully structured-coated conductors, i.e., they have both silver and copper protective coatings on top of the superconducting layer. As a third sample, we consider a YBCO 12 mm wide tape with  $Y_2O_3$  inclusions from SuperOx (batch #ST-12-450-400) produced by PLD on IBAD. In this case, we acquired data both on a piece of sample with a silver protective coating (in the following SuperOx WS) and on a piece without any protective cap so that the superconducting layer is directly exposed (in the following SuperOx NS).

## 2.2. Experimental Details

In this work, we carried out extensive magnetoresistance measurements across a wide range of temperatures and magnetic fields, with the fields oriented both parallel ( $B^{\parallel}$ ) and perpendicular ( $B^{\perp}$ ) to the surface of the coated conductors. We employed a Cryogen Free Magnet (CFM) system from Cryogenic, Ltd. (Cryogenic Limited, Head Office: Unit 6, Acton Park Industrial Estate, The Vale, London W3 7QE, UK) featuring a variable temperature insert and an 18 T superconducting magnet at ENEA Frascati Research Center, whereas a CFM system equipped with a 16 T superconducting magnet at MaSTeR-Lab in CNR-SPIN Salerno. For the SuNAM and SST tapes, the connections were made using a low-melting solder alloy without exposing the superconducting layer. For the SuperOx tape, two pieces were considered. On one of these pieces (SuperOx NS), we removed the protective coating layer by a catalytic process to expose the superconducting layer. The other piece (SuperOx WS) has the silver coating on top of the superconducting layer. On both pieces, we prepared the connections by using silver paste.

The measurements were conducted using a bias current of 40 mA for the SuNAM and SST samples and 10 mA for both the SuperOx pieces, optimizing the tape configuration to maximize the Lorentz force. The resistance as a function of temperature and magnetic field was measured using a standard four-probe technique, with connection configurations as illustrated in the pictures of the samples reported in Figures 1 and 3.

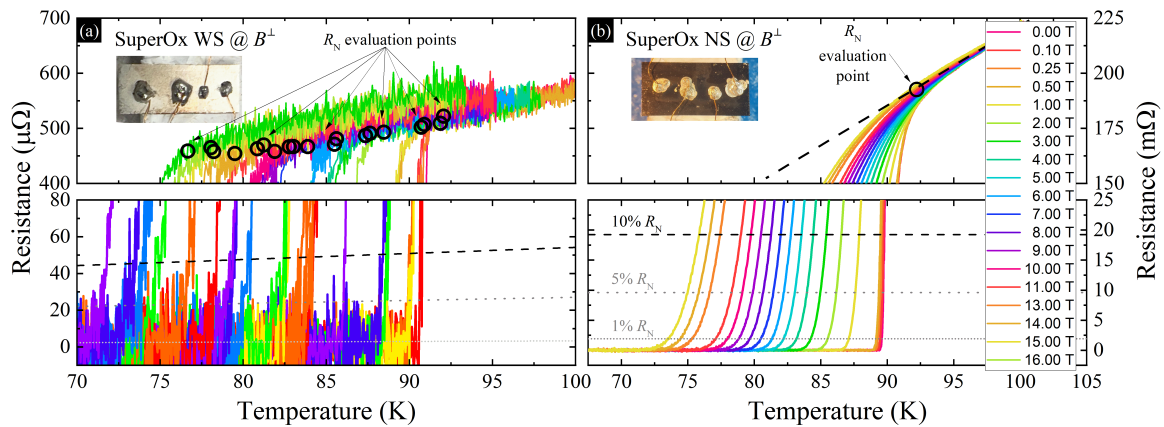


**Figure 1.** Selection of the resistance measurements as a function of temperature at different applied magnetic fields for field applied perpendicularly for the piece of the SuperOx sample with silver coating (a) and the piece without any coating (b). In the upper panels, they are marked with open circles the points at which the normal state resistance value is evaluated. In the lower panels, the lines corresponding to 1%, 5%, and 10% of  $R_N$  criteria are shown on top of the data.

### 3. Results & Discussions

#### 3.1. Criteria Choice

A crucial parameter for real-world applications is the irreversibility field ( $B_{irr}$ ). This is the critical field above which vortices become unpinning and free to move, causing dissipations even under a small current bias. To analyze this parameter from the point of view of practical implementation, we estimated the irreversibility field both parallel  $B_{irr}^{\parallel}$  and perpendicular  $B_{irr}^{\perp}$  to the CCs surface using resistivity measurements. The  $B_{irr}$  values can vary depending on the measurement techniques used, such as probing different physical quantities like magnetic moment or electric field-current density,  $E - J$ , characteristics. Additionally, the criteria applied for these measurements can also affect the  $B_{irr}$  values obtained [44]. In this work, we estimate the irreversibility field from resistance measurements as a function of the temperature,  $R(T)$ . We define the normal state resistance  $R_N$  as the resistance value where the experimental data begin to deviate from linear behavior, as shown in Figure 3 in the case of the SuperOx sample pieces. In particular, for SuperOx WS, the  $R_N$  estimation is conducted for each set of field data due to the presence of non-superconducting components on top of the superconducting layer, i.e., the silver coating. Indeed, the presence of a metallic layer on top of the superconductor affects resistance measurements in the normal state at low temperatures in a way that the onset of the superconducting transition is shifted toward lower temperature values (see upper panel of Figure 1a). In contrast, for the SuperOx NS piece, we estimate  $R_N$  from the zero-field data since the onset of the superconducting transition is the same regardless of the applied magnetic field, resulting in a fan-shape broadening of the transition itself. In other words, the different shape of the transition (shifted for SuperOx WS, fan-like for SuperOx NS) should be here ascribed to the presence, or absence, of a metallic cap and not to changes in the flux pinning effect of various artificial pinning centers as reported, for example, by Zhang et al. [45].

Once defined the criteria to estimate the normal state resistance in the two different cases of a sample with a metallic layer on top of the superconducting one and the case of a sample without a metallic cap, we proceeded to evaluate the irreversibility field at different temperature values. To ensure our data remained safely above the noise level, we adopted a 10% criterion of the normal state resistance. Since in the SuperOx WS case 1% $R_N$  lines fell well within the noise level, while the line given by the 5% criterion is too close to the noise band (see lower panel of Figure 1a). We opted for a 10% criterion for all the samples for sake of estimation uniformity; that is, we estimated  $B_{irr}$  at 10% $R_N$  also for the piece SuperOx NS. At this point, it is worth nothing that the presence of the metallic

stabilization layer on top of the superconducting layer, as in the case of SuperOx WS, causes a sensible decrease in normal state resistance compared with that of a bare sample such as SuperOx NS. As a result, the same criterion corresponds to actual different threshold values. Anyway, it can be seen in Figure 2a that the  $B_{\text{irr}}(T)$  curves obtained for SuperOx NS and SuperOx WS with the 10% criterion follow the same behavior. Further confirmation comes from the comparison of the anisotropy factor  $\gamma_{\text{irr}}$  behaviors. Given that  $\gamma_{\text{irr}}$  is defined as the ratio between  $B_{\text{irr}}^{\parallel}$  and  $B_{\text{irr}}^{\perp}$ , in Figure 2b it is shown that the  $\gamma_{\text{irr}}(T)$  curves for SuperOx NS and SuperOx WS show similar features. From these results, we can conclude that the presence of a metallic cap does not alter the general behavior of the physical parameters, which are estimated well below the superconducting transition middle point. Thus, in the following, for sake of simplicity, we will refer only to the SuperOx NS piece, which represents a sample in between a coated conductor and the reference thin film.

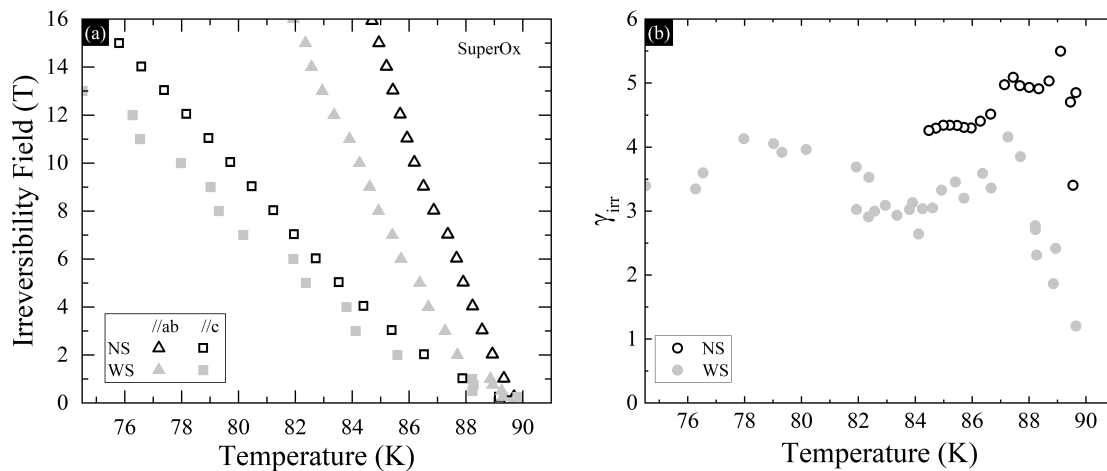


**Figure 2.** Irreversibility Field (a) and its anisotropic factor (b) as function of the temperature for the SuperOx sample: open symbols refer to the NS piece without the silver coating; full symbols refer to the WS piece with silver coating on top of the superconducting layer.

### 3.2. Irreversibility Field

Figure 3 shows a selection of the  $R(T)$  curves for SuNAM, SST, and SuperOx tapes, obtained under varying applied magnetic fields, with the applied magnetic field parallel and perpendicular to the surface of the coated conductor. The results demonstrated that the resistive transition broadens with increasing magnetic field strength in both orientations and shows the anisotropic behavior in the resistive transition. It is worth to recall that SuNAM and SST samples have a metallic stabilization layer on top of the superconducting layer, as in the case of SuperOx WS. Thus, also for SuNAM and SST samples, the onset of the superconducting transition is shifted towards lower temperature as the applied magnetic field increases. Thus, for both SuNAM and SST tapes,  $R_N$  is estimated for each set  $R(T)$  curve. In contrast, for the SuperOx NS sample, we estimate  $R_N$  from the zero-field data as reported previously (Figure 1b).

From data reported in Figure 3b, the resulting  $B_{\text{irr}}$  behaviors for SuNAM and SuperOx NS are evaluated and reported in Figure 4, together with the SST CCs data presented in our recent work [41]. In particular, we can observe the temperature dependence of the irreversibility field anisotropy parameter  $\gamma_{\text{irr}}$ . This is an important parameter to be considered, since a too high value ( $>10$ ) typical of highly anisotropic materials such as BiSCCO requires special attention when designing devices in which the orientation of the magnetic field with respect to the tape cannot be fixed along the whole conductor (e.g., magnets for particle accelerators) [24,27]. Once  $\gamma_{\text{irr}}$  data are reported as a function of the reduced temperature  $t = T/T_c$ , with  $T_c$  being the critical temperature evaluated at 50% of  $R_N$  for each  $R(T, H)$  curve, the three tapes show not that different behaviors. In particular, in the case of SST, the anisotropy is almost constant around a value of 4 with just

a slight increase near  $t = 1$ , while for SuNAM and for SuperOx it is almost constant for  $t < 1$ , but with higher values. Anyway, the values of  $\gamma_{\text{irr}}$  are always well below the typical values for high anisotropic superconductors for all three tapes, which can be then defined as moderately anisotropic CCs.

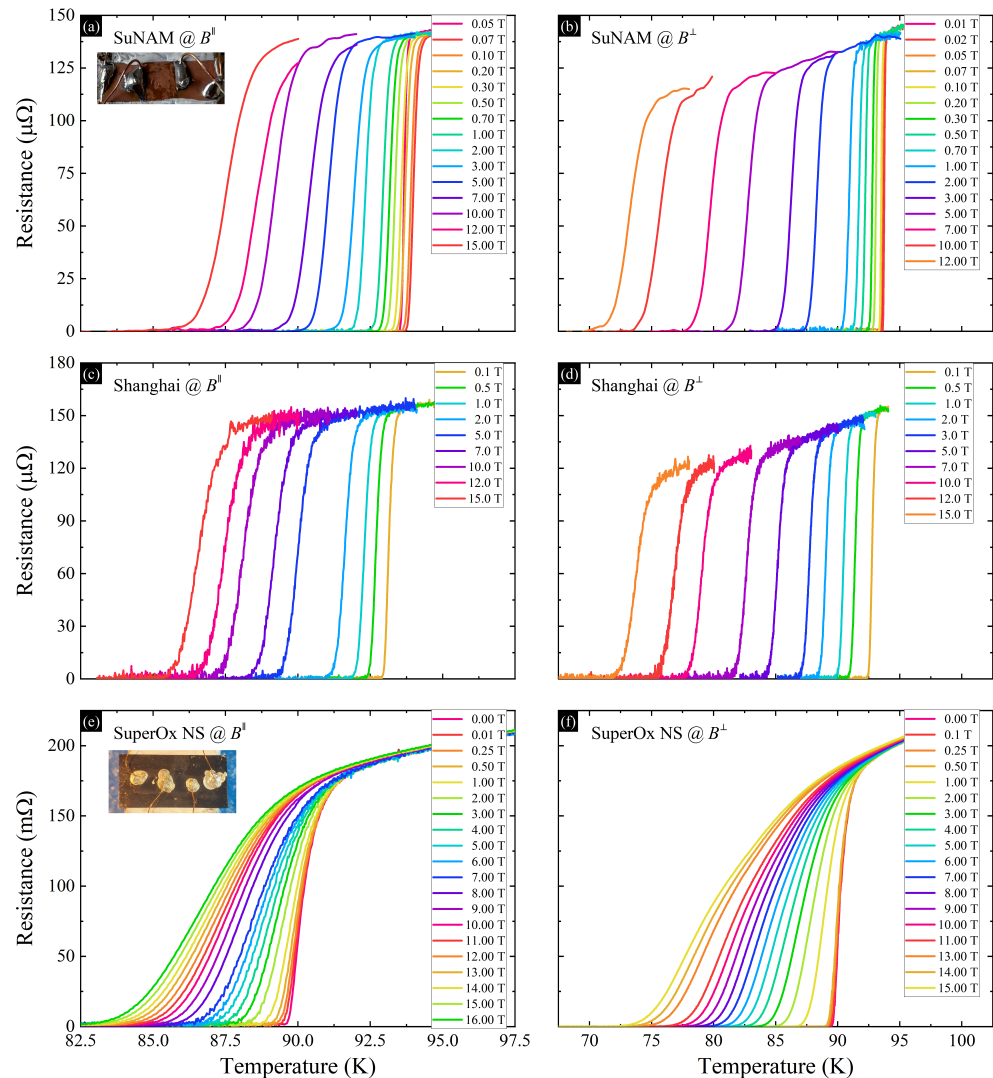


**Figure 3.** Selection of the resistance measurements as a function of temperature at different applied magnetic fields for field applied parallel (a,c,e), and perpendicular (b,d,f) to the tape surface of SuNAM (a,b), SST (c,d), and SuperOx NS (e,f), respectively. In panel (a), the SuNAM sample is shown with the electrical connections realized on top of the metallic stabilization layer. In panel (e), the same for the SuperOx NS piece, but with wires connected directly to the superconducting layer. SST sample looks very similar to SuNAM since electrical connections are soldered on the metallic layer as well.

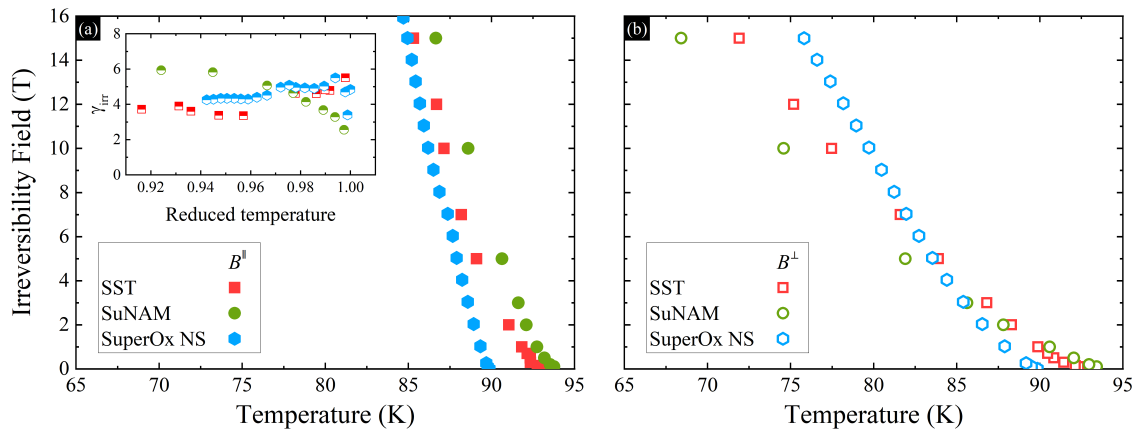


**Figure 4.** Irreversibility field along directions (a) parallel and (b) perpendicular to the CCs surface for both SuNAM and SuperOx samples in comparison with the SST data extracted from [41]. Inset in (a) shows the comparison of the irreversibility field anisotropic parameter behavior as a function of the reduced temperature for the three samples.

### 3.3. Flux Pinning Energy

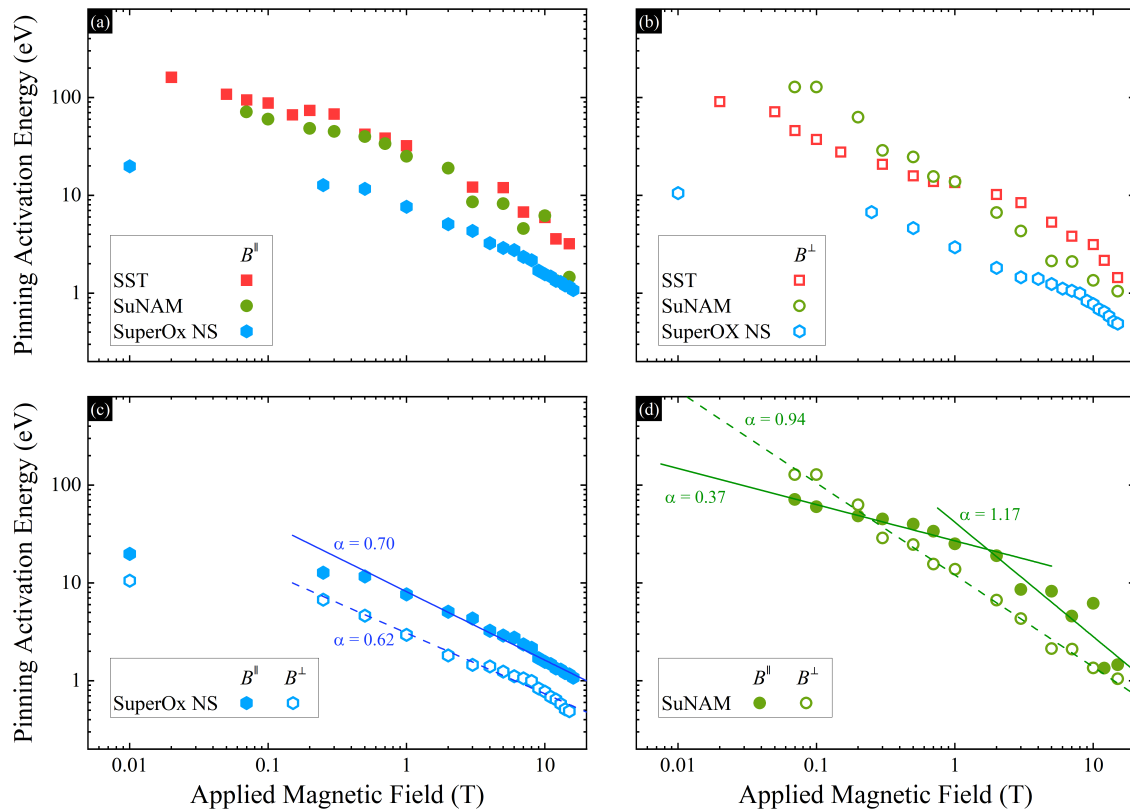
For a superconductor below its transition temperature, the resistance can be described by the equation  $R(T, B, J) = R_0 \exp[U(T, B, J)/k_B T]$ , where  $k_B$  is the Boltzmann constant. With a fixed current density  $J$ , the flux pinning energy  $U(T, B)$  can be estimated using an Arrhenius plot, which involves plotting the logarithm of the resistance against the inverse of the temperature. Therefore, flux pinning energy as a function of the applied magnetic field can be derived by analyzing the  $R(T)$  curves at various magnetic fields using Tinkham's model [46]. According to this approach,  $U$  can be factorized  $U(T, B) = U_0(B)g(t)$ , with  $g(t) = (1 - t^2)(1 - t^4)^{1/2}$ .

Figure 5 illustrates the relationship between the obtained flux pinning energy and the applied magnetic field along parallel ( $U^{\parallel}$ ) and perpendicular ( $U^{\perp}$ ) to the CCs surface of SuNAM, SST, and SuperOx samples. The flux pinning energy is always higher when the magnetic field is applied parallel to the tape surface apart for the SuNAM tape. Although for both SuperOx and SST CCs the flux pinning energy trend is almost the same regardless of applied field orientation, for the SuNAM tape an unexpected crossover occurs around 0.2 T, as it can be appreciated in the panel (d) of Figure 5.

By standard modeling the magnetic field dependence of  $U$  as a power law  $U(B) \propto B^{-\alpha}$  [47], the exponent  $\alpha$  indicates the vortex pinning regime actually operating in the specific field range. Generally, at higher magnetic fields, the vortex spacing becomes much smaller than the penetration depth, leading to a decrease in the flux pinning energy. Indeed, even a faster decrease in  $U$  is observed in the case of SuNAM tape, reaching an exponent  $\alpha$  larger than 1 at high fields, as sometimes found in HTS materials [42,43], which marks a collective vortex pinning regime with strong vortex interactions. On the other hand, it is very well established that  $\alpha$  value close to zero is the signature of a single vortex pinning regime [48,49], which indeed is strictly achieved here only in the case of SuNAM tape for the field direction parallel to the sample surface. Instead, in the case of the SuperOx sample, a hint of a single vortex pinning regime at low field can be noted for both field orientations.

A more detailed comparison among all three tapes can be performed by looking at this flux pinning energy anisotropy by introducing an additional parameter, defined as  $\gamma_U = U^{\parallel}/U^{\perp}$  that is plotted in Figure 6, together with the same parameter evaluated for a plain YBCO film. In this case, the three samples show slightly different behaviors. Figure 6a shows the  $\gamma_U$  behavior for the SST sample; it can be seen that at high field (>5 T), the anisotropy value oscillates around a value of 2. A similar behavior is observed for sample SuperOx, but with a  $\gamma_U$  oscillating around a slightly higher value (Figure 6c). It is worth mentioning that in SuNAM tape, a larger variation of the anisotropy can be expected due to the unexpected crossing occurring between the  $U^{\parallel}$  and the  $U^{\perp}$ , as shown in Figure 5.

Indeed, for SuNAM tape,  $\gamma_U$  first increases from 2 to 3 as the field approaches about 5 T, suddenly decreasing to about 1.5 at higher magnetic fields. Looking at the variations in  $\gamma_U$  of the different tapes with respect to that of the YBCO plain film, it can be noted that in the case of the tapes, trends that are different from the increasing trend of the plain film are shown. Although the  $\gamma_U(H)$  trends for the tapes are not pronounced, it can be drawn that regardless of the nature of Artificial Pinning Centers, i.e., customized or naturally grown, they affect the anisotropy of the pinning landscape in a way that, by increasing the applied magnetic field, a decrease of the  $\gamma_U$  value can be achieved. Thus, there is still room for improving performance by reducing pinning anisotropy by means of proper engineering of APC in the tapes.



**Figure 5.** Flux pinning energy as function of magnetic field applied parallel (a) and perpendicular (b) to the CCs surface for all samples under investigation. SST data are extracted from [41]. The fitting curves with the specific  $\alpha$  values obtained for SuperOx and SuNAM samples are displayed in the panels (c,d), respectively.

Comparing  $\gamma_U$  and  $\gamma_{irr}$ , we must observe that  $\gamma_U$  values are analyzed as a function of the applied magnetic field, while the  $\gamma_{irr}$  are reported as a function of temperature. Anyway, also in the case of  $\gamma_U$ , we can recognize small values of the parameter in the whole considered range of field, thus confirming the moderate anisotropy of the pinning in all three samples, with SuperOx and SST tapes showing the most robust anisotropy against field changes.

A deeper analysis of the flux pinning energy behavior, in particular of its anisotropy  $\gamma_U$ , would require an explicit analytical relation with the anisotropy of the irreversibility field and that of the critical current. Unfortunately, such an explicit relation is still lacking in literature. Such an analysis is beyond the scope of the present work, but it could improve our knowledge on the superconducting properties of the commercial tapes, each one produced by its own fabrication process, with or without artificial pinning centers included, and with a chemical composition strictly related to a proper choice of each manufacturer.

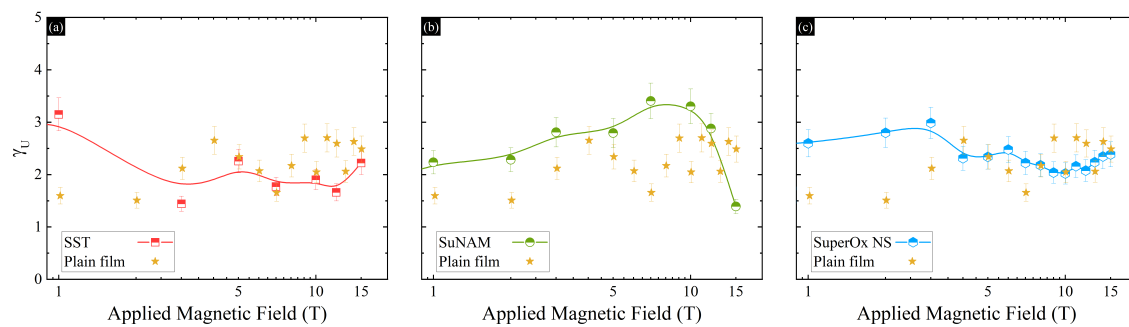


**Figure 6.** Flux pinning energy anisotropy factor  $\gamma_U$  as function of magnetic field for (a) SST, (b) SuNAM, and (c) SuperOx samples compared with that of a YBCO plain film (yellow stars). Error bars are estimated as 10% of the estimated  $\gamma_U$  value.

#### 4. Conclusions

In conclusion, from the general point of view of the pinning anisotropy that becomes a critical parameter in choosing the superconducting tape suitable for a specific application, it is relevant not only looking at the irreversibility field anisotropy but also to the flux pinning energy anisotropy trend. Since the former gives information on the temperature window in which the tape can be operative, the latter can offer the magnetic field range of best performance. In the present work, three different REBCO coated conductors produced by SuperOx, SuNAM Co., Ltd., and Shanghai Superconductors Technology Co., Ltd. have been analyzed. We found that all three samples can be considered moderately anisotropic conductors, although with some slight differences. Indeed, all three samples show variations of the anisotropy factor for the irreversibility field as a function of the temperature. In the case of the flux pinning energy anisotropy, the SST and SuperOx samples show the most resilient behavior against field variations, while the SuNAM sample shows a more complex behavior. Our findings lead to the conclusion that there is still room to strengthen pinning resilience against high temperature and magnetic field through APCs, regardless of the native or external nature of engineered APC.

**Author Contributions:** Conceptualization, A.L., A.N., and G.G.; Data curation, A.L., A.M.; Formal analysis, M.R.K., A.L., A.G., A.N., and G.G.; Funding acquisition, A.N. and G.G.; Investigation, M.R.K., A.L., and A.M.; Methodology, A.L., A.M., A.A., G.C., A.N., and G.G.; Software, A.L.; Supervision, A.N. and G.G.; Validation, A.L., A.M., A.A.A., A.N., and G.G.; Visualization, M.R.K., A.M., A.A.A., and G.G.; Writing—original draft, M.R.K., A.L., A.N., and G.G.; Writing—review and editing, A.G., M.P., G.C., and A.A. All authors have read and agreed to the published version of the manuscript.

**Funding:** This work was supported in part by PON Research and Competitiveness 2007–2013 under Grant PON NAFASSY, PONa3\_00007, and in part by MUR—PRIN 2022 PNRR Project QUESTIONS Grant No. P2022KWFBH. G.G., A.G., and M.P. also acknowledge the EU COST Actions CA19108 Hi-SCALE. M.R. Khan acknowledges financial support by the IRIS Project funded by MUR under contract IR0000003.

**Institutional Review Board Statement:** Not applicable.

**Informed Consent Statement:** Not applicable.

**Data Availability Statement:** The data underlying this article will be shared on reasonable request from the corresponding author.

**Conflicts of Interest:** The authors declare no conflict of interest.

## References

1. Obradors, X.; Puig, T. Coated conductors for power applications: Materials challenges. *Supercond. Sci. Technol.* **2014**, *27*, 044003. [CrossRef]
2. Weijers, H.W.; Markiewicz, W.D.; Voran, A.J.; Gundlach, S.R.; Sheppard, W.R.; Jarvis, B.; Johnson, Z.L.; Noyes, P.D.; Lu, J.; Kandel, H.; et al. Progress in the development of a superconducting 32 T magnet with REBCO high field coils. *IEEE Trans. Appl. Supercond.* **2013**, *24*, 1–5. [CrossRef]
3. Larbalestier, D.C.; Jiang, J.; Trociewitz, U.P.; Kametani, F.; Scheuerlein, C.; Dalban-Canassy, M.; Matras, M.; Chen, P.; Craig, N.C.; Lee, P.J.; et al. Isotropic round-wire multifilament cuprate superconductor for generation of magnetic fields above 30 T. *Nat. Mater.* **2014**, *13*, 375–381. [CrossRef] [PubMed]
4. Zhou, Y.H.; Park, D.; Iwasa, Y. Review of progress and challenges of key mechanical issues in high-field superconducting magnets. *Natl. Sci. Rev.* **2023**, *10*, nwad001. [CrossRef]
5. Boiko, O.; Kwoka, R., Recent Developments in Superconducting Materials Used to Build Short-Circuit Current Limiters, Superconductivity & Particle Accelerators SPAS-2024 Conference. Available online: [https://indico.ifj.edu.pl/event/904/contributions/4735/attachments/1967/3674/Poster%20SPAS-2024\\_O.%20Boiko.pdf](https://indico.ifj.edu.pl/event/904/contributions/4735/attachments/1967/3674/Poster%20SPAS-2024_O.%20Boiko.pdf) (accessed on 18 November 2024).
6. Martucciello, N.; Giubileo, F.; Grimaldi, G.; Corato, V. Introduction to the focus on superconductivity for energy. *Supercond. Sci. Technol.* **2015**, *28*, 070201. [CrossRef]
7. Grimaldi, G.; Bauer, M.; Kinder, H. Continuous reel-to-reel measurement of critical currents of coated conductors. *Appl. Phys. Lett.* **2001**, *79*, 4390–4392. [CrossRef]
8. Senatore, C.; Bonura, M.; Bagni, T. REBCO tapes for applications in ultra-high fields: Critical current surface and scaling relations. *Supercond. Sci. Technol.* **2024**, *37*, 115013. [CrossRef]
9. Puig, T.; Gutierrez, J.; Obradors, X. Impact of high growth rates on the microstructure and vortex pinning of high-temperature superconducting coated conductors. *Nat. Rev. Phys.* **2024**, *6*, 132–148. [CrossRef]
10. Jiang, G.; Zhao, Y.; Zhu, J.; Hong, Y.; Chen, C.; Chen, S.; Wu, Y.; Zhen, S.; Yao, L.; Hong, Z.; et al. Recent development and mass production of high Je 2G-HTS tapes by using thin hastelloy substrate at Shanghai Superconductor Technology. *Supercond. Sci. Technol.* **2020**, *33*, 074005. [CrossRef]
11. Lee, S.; Petrykin, V.; Molodyk, A.; Samoilnikov, S.; Kaul, A.; Vavilov, A.; Vysotsky, V.; Fetisov, S. Development and production of second-generation high Tc superconducting tapes at SuperOx and first tests of model cables. *Supercond. Sci. Technol.* **2014**, *27*, 044022. [CrossRef]
12. Kaul, A.R.; Samoilnikov, S.V.; Amelichev, V.A.; Blednov, A.V.; Kamenev, A.A.; Mankevich, A.S.; Markelov, A.V.; Makarevich, A.M.; Shchukin, A.E.; Kalitka, V.S.; et al. MOCVD buffer and superconducting layers on non-magnetic biaxially textured tape for coated conductor fabrication. *IEEE Trans. Appl. Supercond.* **2013**, *23*, 6601404. [CrossRef]
13. Norton, D.P.; Goyal, A.; Budai, J.D.; Christen, D.K.; Kroeger, D.M.; Specht, E.D.; He, Q.; Saffian, B.; Paranthaman, M.; Klabunde, C.E.; et al. Epitaxial YBa<sub>2</sub>Cu<sub>3</sub>O<sub>7</sub> on Biaxially Textured Nickel (001): An Approach to Superconducting Tapes with High Critical Current Density. *Science* **1996**, *274*, 755–757. [CrossRef]
14. Boffa, V.; Annino, C.; Bettinelli, D.; Ceresara, S.; Ciontea, L.; Fabbri, F.; Galluzzi, V.; Gambardella, U.; Celentano, G.; Grimaldi, G.; et al. Epitaxial growth of heterostructures on biaxially textured metallic substrates for YBa<sub>2</sub>Cu<sub>3</sub>O<sub>7-x</sub> tape fabrication. *Philos. Mag. Part B* **2000**, *80*, 979–990. [CrossRef]
15. Foltyn, S.R.; Civale, L.; MacManus-Driscoll, J.L.; Jia, Q.X.; Maiorov, B.; Wang, H.; Maley, M. Materials science challenges for high-temperature superconducting wire. *Nat. Mater.* **2007**, *6*, 631–642. [CrossRef] [PubMed]
16. Bartolomé, E.; Alcalà, J.; Vallés, F.; Puig, T.; Obradors, X.; Pompeo, N.; Alimenti, A.; Torokhtii, K.; Rizzo, F.; Augieri, A.; et al. Vortex pinning properties at dc and microwave frequencies of YBa<sub>2</sub>Cu<sub>3</sub>O<sub>7-x</sub> films with nanorods and nanoparticles. *Supercond. Sci. Technol.* **2020**, *33*, 074006. [CrossRef]
17. Gao, P.; Zhang, Y.; Wang, X.; Zhou, Y. Interface properties and failures of REBCO coated conductor tapes: Research progress and challenges. *Superconductivity* **2023**, *2023*, 100068. [CrossRef]
18. Pratap, R.; Majkic, G.; Galstyan, E.; Mohanasundaram, G.; Chakradhar, S.; Selvamanickam, V. Growth of high-performance thick film REBCO tapes using advanced MOCVD. *IEEE Trans. Appl. Supercond.* **2019**, *29*, 1–5. [CrossRef]
19. Erbe, M.; Cayado, P.; Freitag, W.; Ackermann, K.; Langer, M.; Meledin, A.; Hänisch, J.; Holzapfel, B. Comparative study of CSD-grown REBCO films with different rare earth elements: Processing windows and Tc. *Supercond. Sci. Technol.* **2020**, *33*, 094002. [CrossRef]
20. Wang, K.; Dong, H.; Huang, D.; Shang, H.; Xie, B.; Zou, Q.; Zhang, L.; Feng, C.; Gu, H.; Ding, F. Advances in second-generation high-temperature superconducting tapes and their applications in high-field magnets. *Soft Sci.* **2022**, *2*, 12. [CrossRef]
21. Paidpilli, M.; Venkat, S. Development of RE-Ba-Cu-O superconductors in the US for ultra-high field magnets. *Supercond. Sci. Technol.* **2022**, *35*, 043001. [CrossRef]
22. Moyzykh, M.; Gorbunova, D.; Ustyuzhanin, P.; Sotnikov, D.; Baburin, K.; Maklakov, A.; Magommedov, E.; Shumkov, A.; Telnova, A.; Shcherbakov, V.; et al. First Russian 220 kV superconducting fault current limiter (SFCL) for application in city grid. *IEEE Trans. Appl. Supercond.* **2021**, *31*, 1–7. [CrossRef]

23. MacManus-Driscoll, J.L.; Wimbush, S.C. Processing and application of high-temperature superconducting coated conductors. *Nat. Rev. Mater.* **2021**, *6*, 587–604. [[CrossRef](#)]
24. Mele, P.; Prassides, K.; Tarantini, C.; Palau, A.; Badica, P.; Jha, A.K.; Endo, T. (Eds.) *Superconductivity: From Materials Science to Practical Applications*; Springer: Berlin, Germany, 2020.
25. Yao, C.; Ma, Y. Superconducting materials: Challenges and opportunities for large-scale applications. *IScience* **2021**, *24*, 102541. [[CrossRef](#)]
26. Marchionini, B.G.; Yamada, Y.; Martini, L.; Ohsaki, H. High-Temperature Superconductivity: A Roadmap for Electric Power Sector Applications, 2015–2030. *IEEE Trans. Appl. Supercond.* **2017**, *27*, 0500907. [[CrossRef](#)]
27. Uglietti, D. A review of commercial high temperature superconducting materials for large magnets: From wires and tapes to cables and conductors. *Supercond. Sci. Technol.* **2019**, *32*, 053001. [[CrossRef](#)]
28. Collomb, D.; Zhang, M.; Yuan, W.; Bending, S.J. Imaging of strong nanoscale vortex pinning in GdBaCuO high-temperature superconducting tapes. *Nanomaterials* **2021**, *11*, 1082. [[CrossRef](#)]
29. Lao, M.; Willa, R.; Meledin, A.; Rijckaert, H.; Chepikov, V.; Lee, S.; Petrykin, V.; Driessche, I.V.; Molodyk, A.; Holzapfel, B. In-field performance and flux pinning mechanism of pulsed laser deposition grown BaSnO<sub>3</sub>/GdBa<sub>2</sub>Cu<sub>3</sub>O<sub>7-δ</sub> nanocomposite coated conductors by SuperOx. *Supercond. Sci. Technol.* **2019**, *32*, 094003. [[CrossRef](#)]
30. Zheng, Y.; Zheng, J.; Wang, X.; Lu, Y. Gamma radiation effects on high-temperature superconducting ReBCO tape. *Supercond. Sci. Technol.* **2024**, *37*, 045013. [[CrossRef](#)]
31. Pęczkowski, P.; Zalecki, R.; Zachariasz, P.; Szostak, E.; Piętosa, J.; Turek, M.; Pyszniak, K.; Zając, M.; Czub, J.; Gondek, Ł. Deterioration of the 2G HTS tapes by the Ne<sup>+</sup> ions irradiation (250 keV). *Appl. Surf. Sci.* **2023**, *636*, 157780. [[CrossRef](#)]
32. Ibragimova, E.M.; Shodiev, A.A.; Ahrorova, S.; Mussaeva, M.A.; Iskandarov, N.E.; Kurbanov, U.T.; Tashmetov, M.Y. Low-dimensional magnetic centers in HTSC YBCO film on steel-276 induced by gamma-quanta and electron beam. *J. Magn. Magn. Mater.* **2024**, *595*, 171617. [[CrossRef](#)]
33. Degtyarenko, P.; Gavrilkin, S.; Tsvetkov, A.; Mineev, N.; Rudney, I.; Ovcharov, A.; Chepikov, V.; Lee, S.; Petrykin, V.; Molodyk, A. The influence of BaSnO<sub>3</sub> artificial pinning centres on the resistive transition of 2G high-temperature superconductor wire in magnetic field. *Supercond. Sci. Technol.* **2020**, *33*, 045003. [[CrossRef](#)]
34. Degtyarenko, P.N.; Ovcharov, A.V.; Vasiliev, A.L.; Chepikov, V.N.; Balashov, N.N.; Degtyarenko, A.Y. Investigation of Pinning and Current-Carrying Capacity in 2G HTS wires with Artificial Pinning Centers obtained at various deposition rates. *IEEE Trans. Appl. Supercond.* **2023**, *33*, 4802506. [[CrossRef](#)]
35. Chepikov, V.; Mineev, N.; Degtyarenko, P.; Lee, S.; Petrykin, V.; Ovcharov, A.; Vasiliev, A.; Kaul, A.; Amelichev, V.; Kamenev, A.; et al. Introduction of BaSnO<sub>3</sub> and BaZrO<sub>3</sub> artificial pinning centres into 2G HTS wires based on PLD-GdBCO films. Phase I of the industrial R&D programme at SuperOx. *Supercond. Sci. Technol.* **2017**, *30*, 124001.
36. Maiorov, B.; Baily, S.A.; Zhou, H.; Ugurlu, O.; Kennison, J.A.; Dowden, P.C.; Holesinger, T.G.; Foltyn, S.R.; Civale, L. Synergetic combination of different types of defects to optimize pinning landscape using BaZrO<sub>3</sub>-doped YBa<sub>2</sub>Cu<sub>3</sub>O<sub>7</sub>. *Nat. Mater.* **2009**, *8*, 398–404. [[CrossRef](#)]
37. Feighan, J.P.F.; Kursumovic, A.; MacManus-Driscoll, J.L. Materials design for artificial pinning centres in superconductor PLD coated conductors. *Supercond. Sci. Technol.* **2017**, *30*, 123001. [[CrossRef](#)]
38. Park, I.; Oh, W.J.; Lee, J.H.; Moon, S.H.; Yoo, S.I. Improvement of Pinning Properties by refining Gd<sub>2</sub>O<sub>3</sub> particles trapped in GdBa<sub>2</sub>Cu<sub>3</sub>O<sub>7-δ</sub> coated conductors fabricated by the RCE-DR process. *IEEE Trans. Appl. Supercond.* **2021**, *31*, 5, 6600605. [[CrossRef](#)]
39. Tsuchiya, K.; Wang, X.; Fujita, S.; Ichinose, A.; Yamada, K.; Terashima, A.; Kikuchi, A. Superconducting properties of commercial REBCO-coated conductors with artificial pinning centers. *Supercond. Sci. Technol.* **2021**, *34*, 105005. [[CrossRef](#)]
40. Senatore, C.; Barth, C.; Bonura, M.; Kulich, M.; Mondonico, G. Field and temperature scaling of the critical current density in commercial REBCO coated conductors. *Supercond. Sci. Technol.* **2016**, *29*, 014002. [[CrossRef](#)]
41. Khan, M.R.; Leo, A.; Masi, A.; Pinto, V.; Armenio, A.A.; Augieri, A.; Celentano, G.; Martucciello, N.; Nigro, A.; Grimaldi, G. Characterization of Critical Fields and Flux Pinning Energy of REBCO Tapes. *IEEE Trans. Appl. Supercond.* **2024**, *34*, 6602505. [[CrossRef](#)]
42. Guarino, A.; Leo, A.; Grimaldi, G.; Martucciello, N.; Dean, C.; Kunchur, M.N.; Pace, S.; Nigro, A. Pinning mechanism in electron-doped HTS Nd<sub>1.85</sub>Ce<sub>0.15</sub>CuO<sub>4-δ</sub> epitaxial films. *Supercond. Sci. Technol.* **2014**, *27*, 124011. [[CrossRef](#)]
43. Galluzzi, A.; Crisan, A.; Ionescu, A.M.; Ivan, I.; Leo, A.; Grimaldi, G.; Polichetti, M. Pinning energy and evidence of granularity in the AC susceptibility of an YBa<sub>2</sub>Cu<sub>3</sub>O<sub>7-x</sub> superconducting film. *Appl. Sci.* **2024**, *14*, 4379. [[CrossRef](#)]
44. Grimaldi, G.; Khan, M.R.; Leo, A.; Scuderi, M.; Rizzo, F.; Augieri, A.; Celentano, G.; Galluzzi, A.; Iebole, M.; Polichetti, M.; et al. Unveiling intrinsic material and extrinsic pinning dimensionality in superconductors: Why Fe(Se,Te) is able to mimic YBCO. *iScience* **2024**, *27*, 109422. [[CrossRef](#)]
45. Zhang, Y.Q.; Xiang, X.Q.; Ding, J.F.; Li, X.G. The crossover from parallel shift to fan-shape broadening of the superconducting transition of La<sub>1.44</sub>Nd<sub>0.4</sub>Sr<sub>0.16</sub>CuO<sub>4</sub> films in magnetic fields. *Supercond. Sci. Technol.* **2008**, *21*, 095005. [[CrossRef](#)]
46. Tinkham, M. Resistive transition of high-temperature superconductors. *Phys. Rev. Lett.* **1988**, *61*, 1658. [[CrossRef](#)]
47. Blatter, G.; Feigel'Man, M.V.; Geshkenbein, V.B.; Larkin, A.I.; Vinokur, V.M. Vortices in high-temperature superconductors. *Rev. Mod. Phys.* **1994**, *66*, 1125–1388. [[CrossRef](#)]

48. Scuderi, M.; Pallecchi, I.; Leo, A.; Nigro, A.; Grimaldi, G.; Ferdeghini, C.; Spinella, C.; Guidolin, M.; Trotta, A.; Braccini, V. Nanoscale analysis of superconducting Fe(Se,Te) epitaxial thin films and relationship with pinning properties. *Sci. Rep.* **2021**, *11*, 20100. [[CrossRef](#)]
49. Khan, M.R.; Leo, A.; Nigro, A.; Galluzzi, A.; Polichetti, M.; Braccini, V.; Cialone, M.; Scuderi, M.; Grimaldi, G. Effective magnetic field dependence of the flux pinning energy in FeSe<sub>0.5</sub>Te<sub>0.5</sub> superconductor. *Materials* **2021**, *14*, 5289. [[CrossRef](#)]

**Disclaimer/Publisher's Note:** The statements, opinions and data contained in all publications are solely those of the individual author(s) and contributor(s) and not of MDPI and/or the editor(s). MDPI and/or the editor(s) disclaim responsibility for any injury to people or property resulting from any ideas, methods, instructions or products referred to in the content.